IAC-18,A6,IP,31,x42794

Prospects of Touchless Space Debris Detumbling Using an Electrostatic Pusher Configuration

Vladimir Aslanov[a] **and Hanspeter Schaub**[b]

[a] Professor, Samara National Research University, Russian Federation, aslanov vs@mail.ru
[b] Professor, Glenn L. Murphy Chair of Engineering, Department of Aerospace Engineering Sciences, University of Colorado, 431 UCB, Colorado Center for Astrodynamics Research, Boulder, CO 80309-0431, hanspeter.schaub@colorado.edu

Abstract. The relative attitude motion is studied between two charge controlled geosynchronous bodies being held at a predetermined along-track configuration. While body one, the space tug, is modeled with a spherical shape, the 2nd body, the large space debris, is assumed to be cylindrical and tumbling. This scenario allows for simultaneous repositioning and detumbling of both large and small GEO space objects. Detumbling is critical for orbital servicing where rotational motions above one degree per second prohibit current docking solutions. This paper focuses on challenges particular to a pusher configuration where the debris and tug have nominally the same charge. A Multi-Sphere Method approach is investigated to model the electrostatic forces and torques. Using a first-order expansion new electrostatic torque predictions are incorporated into the detumble feedback control component. Multiple even and odd control solutions are hypothesized and their linearized stability properties discussed. Only in-plane relative motion of the tug and debris are considered to focus on planar relative heading control and the impact of the MSM modeling within the control formulation. Numerical simulations illustrate how the parameters of the bodies and the control impact the stability of the system.
Keywords
Space debris, Space tug, Coulomb force, Relative motion, Control, Stabilization

Nomenclature

m_1 = mass of the tug, kg

m_2 = mass of the debris, kg

J = moment of inertia of the space debris, kg m^2

$k_c = 8.99 \times 10^9 \, Nm^2 / C^2$ = Coulomb's constant

$C_1 xy$ = Local-Vertical-Local-Horizontal (LVLH) coordinate

θ = pitch attitude angle

θ_s = stable equilibrium position

θ_u = unstable equilibrium position

α = angle between local horizontal line of the tug and the line connecting the tug and debris, rad

$\mathbf{d}$ = position vector of the debris relative to the space tug, m

$d = |\mathbf{d}| $ = distance between the space tug and debris, m

$\mathbf{r}_i$ = position vector of the space tug ($i = 1$) and debris ($i = 2$), m

m_i = mass of the space tug ($i = 1$) and debris ($i = 2$), kg \

n = mean motion of the space tug, $1 / s$

$\mathbf{e}_x$ = unit vector of the local vertical at the space tug position, m

$\mathbf{e}_y$ = unit vector of the local horizontal at the space tug position, m

$\mathbf{F}_i$ = net force acting on the space tug ($i = 1$) and debris ($i = 2$), N

$\mathbf{F}_{1,2}$ = Coulomb force acting on the debris, N

$\mathbf{F}_{2,1}$ = Coulomb force acting on the space tug, N

$\mathbf{D}_i$ = sum of the perturbation forces acting on the space tug ($i = 1$) and debris ($i = 2$), N

U_x, U_y = projections of the control force, N

u_x, u_y = projections of the accelerations provided by the control forces U_x and U_y, m/s^2

$\mathbf{P}$ = is the tug's thrust force vector, N

a_p = acceleration of the space tug provided by the thrust force P, m/s^2

c_α = feedback control coefficient, m/s^2

c_ω = feedback control coefficient, m/s

c_v = feedback control coefficient $1/s$

q_i = craft charges ($i = 1$ for the space tug and $i = 2$ for the debris), C

k_e = Coulomb constant, $N \cdot m^2 \cdot C^{-2}$

I. Introduction

Space debris is a growing concern for both Leo Earth Orbit (LEO) and Geosynchronous Orbit (GEO) regimes.[1-3]. In particular, the comprehensive study in Reference 2 discusses how zones within the GEO regime are becoming very congested, rivaling the worst LEO debris concerns. The defunct GEO satellites tend to be very large, often reaching beyond 5-10 meter in size, as well as rotating and tumbling.[4]   The act of docking onto such large and tumbling space objects is very challenging, and as a result novel touchless debris removal or despinning solutions are being explored. The ion-shepherd method uses the ion engine exhaust to push and/or despin a satellite[5], while the laser ablation method uses the debris' own mass as a thruster fuel source.[6] A promising touchless and low-power solution is the electrostatic tractor.[7]. Here active charge emission is used to both charge the tug or servicer vehicle as well as the debris object. While the original concept uses an electron gun to charge the tug positive and debris negative, creating an attractive electrostatic tractor force, with auxiliary charge emission on the tug it is also possible to charge both servicer and debris to the same potential to create a repulsive force.[8,9] Most of the control research using the electrostatic tractor considers a pulling configuration to move GEO objects.[10]. Further, modulated electrostatic tractor implementations are studies to detumble a space object without physical touch.[11] This will enable orbital servicing and docking missions to first remove a large amount of the rotational kinetic energy before physically docking and engaging with a satellite.

The aim of this paper is to investigate the control of the space tug and debris for the removal and detumbling of the space debris or defunct satellite using electrostatic forces. The goal is to provide a stable relative motion of the tug and the debris both in terms of translation and rotation. With the spacecraft and debris nominally charged with the same polarity to consider a pusher configuration, a feedback control method using both the thrusters for station-keeping and electrostatic charge modulation of the space tug for pushing and detumbling is considered. The feedback control laws aligns the tug-debris direction with the tug along-track orbit axis and maintains a nominally constant distance between the charged tug and debris, all while stabilizing the attitude motion of the debris. For the scope of this paper only in-plane motion of the tug and debris are considered. The tug is assumed as a sphere with a homogenous potential and the debris as a rigid conducting cylindrical body that have nominal electric charges of the same sign and the repulsive electrostatic forces act between the tug and the debris. Further, the tug has two thrusters: the main thruster, which provides the acceleration of the whole system for the disposal of the debris to a disposal orbit and the control thruster, which ensures the required position of the tug relative to the debris. This scenario covers general repositioning of both large and small GEO satellites, as well as moving large space debris to a disposal orbit which lies to 200-250 km above GEO orbit.

II. Accurate Electrostatic Torque Approximations
A. Multi-Sphere Model Overview

Modeling the electrostatic forces and torques between two three-dimensional conducting shapes is readily solved these days using numerical finite element programs. However, the time to evaluate a single solution can range from a minute to 10's of minutes depending on the complexity of the scenario. To model the dynamics of two neighboring charged space objects these force evaluation times are orders of magnitude too large to be practical. Consider the Geosynchronous Earth Orbit (GEO) regime where natural charging can reach 10's of kilo-Volts with particular space weather conditions. [12-16] To simulate the rotational motion of two charged GEO using a 4th order Runge-Kutta integration method and a 0.1s time step, assuming a conservative 60 seconds per force evaluation, would require a 2400 days of computation time. Faster numerical methods are required to approximate the electrostatic forces and torques acting on a system of charged objects.   The Multi-Sphere Method (MSM) is a lower-fidelity electrostatic modeling technique that can be evaluated quickly enough for faster-than-realtime applications. [17-18]

With MSM the conducting spacecraft charge distribution is modeled through a series of spheres. The optimal locations of these spheres are found through either a force and torque,[19] or an E-field matching technique.[20]

Figure 1 illustrates a cylindrical rocket body being modeled through a set of three internal spheres. This MSM technique is called the Volume MSM or VMSM method. An alternate MSM technique, called the Surface MSM or SMSM method, populates the object's surface with a series of spheres.[18] The SMSM method can yield more accurate approximates then the VMSM models, but the number of spheres makes any analytical formulations impractical. Assuming a 2-3 craft radii separation, either method can yield accuracies that are better than 1-2%.

MSM is an elastance-based method for predicting the force and torque on conductors.[21] With either the VMSM or the SMSM technique the mathematical formulation of the E-forces and torques is the same. Assume the objects are represented through N_T conducting spheres whose optimal body-fixed locations and sizes have been determined apriori. The $N_T \times 1$ charge matrix, $\boldsymbol{q} = [q_1 \quad q_2 \quad \cdots \quad q_{N_T}]$, which contains the charge on each sphere of a MSM model, is related to the $N_T \times 1$ sphere voltage matrix $\boldsymbol{\Phi} = [\Phi_1 \quad \Phi_2 \quad \cdots \quad \Phi_{N_T}]$ through:[17]

$$\boldsymbol{q} = \frac{1}{k_c} C_M \boldsymbol{\Phi} \tag{1}$$

where $k_c = 1/(4\pi\epsilon_0)$ is the Coulomb constant, and the $N_T \times N_T$ matrix $\frac{1}{k_c} C_M$ is the Position Dependent Capacitance (PDC) matrix. The inverse of C_M is the elastance matrix S which is readily formulated as

$$S = k_c \begin{bmatrix} \frac{1}{R_1} & \frac{1}{r_{1,2}} & \cdots & \frac{1}{r_{1,N_T}} \\ \frac{1}{r_{1,2}} & \frac{1}{R_2} & \cdots & \frac{1}{r_{2,N_T}} \\ \vdots & \vdots & \ddots & \vdots \\ \frac{1}{r_{1,N_T}} & \frac{1}{r_{2,N_T}} & \cdots & \frac{1}{R_{N_T}} \end{bmatrix} \tag{2}$$

where R_i are the individual MSM sphere radii and $r_{i,j}$ is the relative distance between spheres i and j. By knowing the potential Φ_i on each sphere, Eqs. (1) and (2) allow for the MSM charges q_i to be computed. The computational speed, or analytical complexity of the charge formulation, is directly dependent on how many MSM spheres are used. The VMSM approach yields good approximations with a small number of spheres for very rapid numerical force evaluations, and some analytical insight if only 2-3 spheres are used. The SMSM model provides enhanced fidelity as it can better model non-homogenous charge distributions if the objects are very close to each other. However, instead of using 2-3 VMSM spheres, the SMSM approach uses 10's or 100's of spheres. As the elastance matrix inverse is an N^3 order evaluation, the SMSM modeling is orders of magnitude slower than VMSM solution, but provides noticeable accuracy improvements if the craft are separated less than 2-3 craft radii.

To evaluate the general forces and torques, the Coulomb interactions are summed up across all the MSM spheres through

$$\boldsymbol{F} = -k_c \sum_{k=1}^{M} q_k \sum_{i=1}^{N} \frac{q_i}{\|r_{i,k}\|^3} \boldsymbol{r}_{i,k} \tag{2}$$

$$\boldsymbol{\tau} = -k_c \sum_{k=1}^{M} q_k \sum_{i=1}^{N} \frac{q_i}{\|r_{i,k}\|^3} \boldsymbol{r}_{i,k} \tag{3}$$

Here the Debye shield of the local plasma environment is ignored as the separation distance considered, 10-25 meters, is significantly less than the average minimum GEO Debye length of 200 meters.

Next, the specific scenario is considered there the MSM modeling is used for a debris-tug scenario as illustrated in Figure 1. Here the tug is modeled through a single sphere C_1 and the cylindrical debris is modeled through three spheres A, B and C_2. The conducting debris object has the potential Φ_D and the conducting spherical tug has the potential Φ_T. The charge voltage relationship is now partitioned as

$$\begin{bmatrix} \Phi_D \\ \Phi_D \\ \Phi_D \\ \Phi_T \end{bmatrix} = k_c \begin{bmatrix} & & & \vdots & \\ & S_D & & \vdots & S_{D,T} \\ & & & \vdots & \\ \cdots & \cdots & \cdots & \cdots & \cdots \\ & S_{D,T}^T & & \vdots & S_T \end{bmatrix} \begin{bmatrix} q_a \\ q_b \\ q_{c_2} \\ \cdots \\ q_{c_1} \end{bmatrix} \tag{4}$$

where the elastance matrix partitions are defined as

$$S_D = \begin{bmatrix} \frac{1}{R_a} & \frac{1}{r_{a,b}} & \frac{1}{r_{a,c_2}} \\ \frac{1}{r_{a,b}} & \frac{1}{R_a} & \frac{1}{r_{b,c_2}} \\ \frac{1}{r_{a,c_2}} & \frac{1}{r_{b,c_2}} & \frac{1}{R_{c_2}} \end{bmatrix} \tag{6a}$$

$$S_{D,T} = \begin{bmatrix} \frac{1}{r_{a,c_1}} & \frac{1}{r_{b,c_1}} & \frac{1}{r_{c_2,c_1}} \end{bmatrix}^T \tag{6b}$$

$$S_T = \begin{bmatrix} \frac{1}{R_{c_1}} \end{bmatrix} \tag{6c}$$

Note that the inverse of S_D and S_T yield the self-capacitance matrix of the debris and tug respectively, while the mutual capacitance between them is the $S_{D,T}$ partition. Using the Schur complement matrix decomposition[22] to express the elastance matrix inverse allows Eq. (5) to be solved for the charges using:

$$\begin{bmatrix} q_a \\ q_b \\ q_{c_2} \end{bmatrix} = \frac{1}{k_c} \left(\Gamma \boldsymbol{\Phi}_D - \Gamma S_{D,T} S_T^{-1} \boldsymbol{\Phi}_T \right) \tag{7a}$$

$$q_{c_1} = \frac{1}{k_c} \left(-S_T^{-1} S_{D,C}^T \Gamma \boldsymbol{\Phi}_D + \left(S_T^{-1} + S_T^{-1} S_{D,C}^T \Gamma S_{D,T} S_T^{-1} \right) \boldsymbol{\Phi}_T \right) \tag{7b}$$

where

$$\Gamma = \left(S_D - S_{D,T} S_T^{-1} S_{D,T}^T \right) \tag{8}$$

and

$$\boldsymbol{\Phi}_D = \begin{bmatrix} \Phi_D & \Phi_D & \Phi_D \end{bmatrix}^T \tag{9}$$

The mutual elastance component $S_{D,T}$ accounts for the fact that two neighboring charged objects will impact each other's charge to voltage relationship. However, if the separation distance grows sufficiently large, this influence becomes negligible. If MSM is used for a feedback control development, then the charge evaluations in Eq. (7) rendered much more complex if this mutual capacitance term is included. If $S_{D,T}$ can be assumed to be small, then the charge equations in Eq. (7) simplify to the two isolated body solutions

$$\begin{bmatrix} q_a \\ q_b \\ q_{c_2} \end{bmatrix} = \frac{1}{k_c} S_D^{-1} \boldsymbol{\Phi}_D \tag{10a}$$

$$q_{c_1} = \frac{1}{k_c} S_T^{-1} \Phi_T \tag{10b}$$

For the particular cylinder (debris) and sphere (tug) scenario illustrated in Figure 1, the total electrostatic force onto the cylinder is then given by [17,19]

$$\mathbf{F}_{E2} = -\mathbf{F}_{E1} = k_c |q_1| \sum_{i=a}^{c} \frac{q_i}{r_i^3} \mathbf{r_i} \tag{11}$$

while the force on each of the cylinder MSM spheres is given by

$$\mathbf{F}_{2,i} = k_c \frac{|q_1| q_i}{r_i^3} \mathbf{r_i}, \qquad i = a, b, c \tag{12}$$
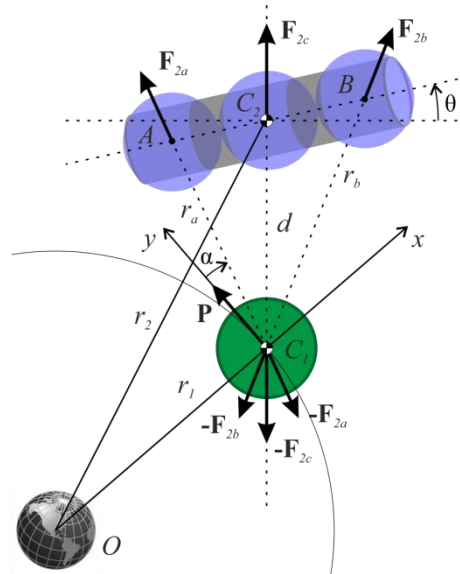
Fig. 1 Multi-Sphere Illustration of a Tumbling Cylinder Neighboring a Spherical Tug

Local-Vertical-Local-Horizontal (LVLH) coordinate frame is used to describe relative motion of two spacecraft. The origin of the LVLH frame is the center of mass of the space tug C_1. Axis C_1x is aligned with the local vertical line and C_1y axis is aligned with the local horizontal line (Fig. 1). We assume that the distance between the bodies is varied $\left(r_b = d = \mathrm{var}\right)$ according to the motion equations of the debris and the tug.

B. Planar Rotational Equations of Motion

Attitude motion. To describe the motion of the debris relative to its own mass center C_2, we use the angular momentum theorem

$$\frac{d}{dt}\left[J\left(\dot{\theta}-\dot{\alpha}+\dot{f}\right)\right]=L_E+L_G \tag{13}$$

Here the electrostatic torque is

$$L_E = \frac{\partial \mathbf{r}_{ca}}{\partial \theta}\cdot \mathbf{F}_{2a} + \frac{\partial \mathbf{r}_{cb}}{\partial \theta}\cdot \mathbf{F}_{2b}, \qquad (\mathbf{r}_{ca}=\overline{CA},\ \mathbf{r}_{cb}=\overline{CB}) \tag{14}$$

and the gravitational torque is

$$L_G = \frac{3n^2}{\left(1-e^2\right)^3}\left(1+e\cos f\right)^3\left(J-J_0\right)\sin\left(\theta-\alpha\right)\cos\left(\theta-\alpha\right) \tag{15}$$

where $J_x = J_y = J_0, J = J_z$ are the moments of inertia of the cylindrical debris object.

The electrostatic torque in Eq. (14) is non-trivial due to the complexity of the determining Coulomb forces in Eq. (11) using the capacitance relation in Eq. (5) and (6), and to obtain analytical solutions the symbolic manipulator MATHEMATICA [23] is used. After some additional transformations the electrostatic torque in Eq. (14) is written as

$$\tag{16}$$

Here

$$H\left(\theta,d\right)=[-4d^2lR_1G_+^2R_2(l^2-R_2R_{2,c})+4dlR_1G_-G_+R_2(2lG_+R_{2,c}+R_2(dl-(2d+G_+)R_{2,c}))+$$
$$G_-^2(4dlR_1G_+(2l-R_2)R_2R_{2,c}-4d^2lR_1R_2(l^2-R_2R_{2,c})+G_+^2(2l-R_2)(2l^2(d^2-R_1R_{2,c})+$$
$$R_2(d^2l-(4d^2+lR_1)R_{2,c})))]^2 \tag{17}$$

$$G_{\pm}\left(\theta,d\right)=\left(l^2\pm 2ld\sin\theta+d^2\right)^{1/2} \tag{18}$$

where $d=\left|\mathbf{r}_2-\mathbf{r}_1\right|=\sqrt{x^2+y^2}$ is the separation distance vector between the objects, θ is the cylinder orientation angle(Fig.1), Φ_1 is the controlled voltages of the tug, Φ is the constant voltages of the debris.

In equation (16) an unimportant assumption is used where $R_{2,b}=R_{2,a}=R_2$ and R_2 is radius of the cylinder 2 (debris).

Motion of the system relative to the inertial frame. At first the motion of the space tug and debris is considered in the Earth-centered inertial (ECI) frame $OXYZ$. The origin of $OXYZ$ frame is in the center of the Earth. The OXY plane coincides with the Earth's equatorial plane, the OX axis is aligned with the equinox, the OZ axis extends through the North Pole. The position of the space tug and space debris described by the column vectors $\mathbf{r}_1=[x_1,y_1]^T$ and $\mathbf{r}_2=[x_2,y_2]^T$ respectively. The inertial equations of motion of the space tug and debris relative to $OXYZ$ frame are:

$$m_i\frac{d^2\mathbf{r}_i}{dt^2}=-\mu\frac{\mathbf{r}_i}{r_i^3}+\mathbf{F}_i,\quad i=1,2 \tag{19}$$

where the time derivatives are inertial derivatives of the vectors, $m_i\ \left(i=1,2\right)$ are masses of the tug $\left(i=1\right)$ and debris $\left(i=2\right)$ objects, $\mathbf{F}_i\ \left(i=1,2\right)$ are the net forces acting on the space tug $\left(i=1\right)$ and debris $\left(i=2\right)$

$$\mathbf{F}_1 = U_x\mathbf{e}_x + (P+U_y)\mathbf{e}_y + \mathbf{F}_{E1} + \mathbf{N}_1 \tag{20}$$
$$\mathbf{F}_2 = \mathbf{F}_{E2} + \mathbf{N}_2 \tag{21}$$

where $\mathbf{N}_i$ is the net vector of other disturbance forces acting on the tug $\left(i=1\right)$ and the debris $\left(i=2\right)$ which include gravity perturbations of the Sun and the Moon, solar pressure and perturbations due to a non-spherical Earth's gravity. $P=\mathrm{const}$ is the nominally constant station-keeping thrust force of the space tug. This thrust $\mathbf{P}$ is assumed to be aligned with the local horizontal axis of the space tug.

The Coulomb forces acting between the objects are defined by Eq. (11)

$$\mathbf{F}_{E1} = -\mathbf{F}_{E2} = -\left(\mathbf{F}_{2a} + \mathbf{F}_{2b} + \mathbf{F}_{2c}\right) \tag{22}$$

These equations are non-trivial due to the complexity of the determining Coulomb forces in Eq. (11) through the elastance and capacitance matrices in Eqs. (5) and (6). To obtain analytical force solutions the symbolic manipulator MATHEMATICA [23] is used. Using Eq. (14) and after performing some additional transformations the Coulomb force in Eq. (22) is written as

$$\mathbf{F}_{E1} = \left(F_{E1,x}, F_{E1,y}\right) = -\frac{1}{H}\left(a_{E,x}\left[b_{E,x}\cos(\alpha-\theta) + c_{E,x}\sin\alpha\right], a_{E,y}\left[b_{E,y}\sin(\alpha-\theta) + c_{E,y}\cos\alpha\right]\right) \tag{23}$$

where the following definitions are used to yield the compact expression in equation (23):

$$a_{E,x}(\theta,d) = \Phi_1 dlR_1(2l - R_2)G_-G_+\left[2l^2 + R_2(l - 4R_{2,c})\right] +$$
$$\Phi_2 lR_1(2l - R_2)\left[lG_-G_+(-2l + 3R_2)R_{2,c} + 2dlG_-R_2(-l + R_{2,c}) + 2dlG_+R_2(-l + R_{2,c})\right]$$

$$b_{E,x}(\theta,d) = \Phi_1 2dl(G_- - G_+)R_2\left[dR_1G_-^3G_+(2l - R_2)R_{2,c} + dR_1G_-^2G_+^2(2l - R_2)R_{2,c} + dR_1G_-G_+^3(2l - R_2)R_{2,c} +\right.$$
$$\left. d^2R_1(lG_-^2G_+(-2l + R_2) + lG_-G_+^2(-2l + R_2)) - 2(G_-^3 + G_+^3)(l^2 - R_2R_{2,c}))\right] +$$
$$\Phi_2 2dl(G_- - G_+)R_2\left[d^2(G_-^3G_+(2l - R_2) + G_-G_+^3(2l - R_2) + 2lR_1G_-^2R_2 + G_-^2(G_+^2(2l - R_2) +\right.$$
$$2lR_1R_2))(l - R_{2,c}) + dlR_1G_-^2G_+(2l - R_2)R_{2,c} - lR_1G_-^3G_+(2l - R_2)R_{2,c} + dlR_1G_-G_+^2(2l - R_2)R_{2,c} -$$
$$\left. lR_1G_-^2G_+^2(2l - R_2)R_{2,c} - lR_1G_-G_+^3(2l - R_2)R_{2,c} - 2dlR_1G_-^3(-l + R_2)R_{2,c} - 2dlR_1G_+^3(-l + R_2)R_{2,c}\right]$$

$$c_{E,x}(\theta,d) = \Phi_1\left[2d^4G_-^3G_+R_1R_2^2(l - 2R_{2,c}) + 2d^4G_-G_+^3R_1R_2^2(l - 2R_{2,c}) + 2d^3G_-^4G_+R_1(2l - R_2)R_2R_{2,c} +\right.$$
$$2dG_-^4G_+^3R_1(2l - R_2)R_2R_{2,c} + 2d^3G_-G_+^4R_1(2l - R_2)R_2R_{2,c} + 2dG_-^3G_+^4R_1(2l - R_2)R_2R_{2,c} -$$
$$\left. G_-^4G_+^4R_1(2l - R_2)(2l + R_2)R_{2,c} - 4d^4G_-^4R_1R_2(l^2 - R_2R_{2,c}) + 4d^4G_+^4R_1R_2(-l^2 + R_2R_{2,c})\right] +$$
$$\Phi_2\left[2d^4G_-^4G_+(2l - R_2)R_2(l - R_{2,c}) + 2d^4G_-G_+^4(2l - R_2)R_2(l - R_{2,c}) + 4d^4lG_-^3R_1R_2^2(l - R_{2,c}) +\right.$$
$$4d^4lG_+^3R_1R_2^2(l - R_{2,c}) + 4d^3lG_-^4R_1(l - R_2)R_2R_{2,c} + 4d^3lG_+^4R_1(l - R_2)R_2R_{2,c} +$$
$$2lG_-^4G_+^3R_1(2l - R_2)R_2R_{2,c} + 2lG_-^3G_+^4R_1(2l - R_2)R_2R_{2,c} - 2d^2lG_-G_+(G_-^3 + G_+^3)R_1(2l - R_2)R_2R_{2,c} +$$
$$2d^3lG_-^3G_+R_1R_2^2R_{2,c} + 2d^3lG_-G_+^3R_1R_2^2R_{2,c} - 4dlG_-^3G_+^3R_1R_2^2R_{2,c} + 4dlG_-^4G_+^2R_1R_2(-l + R_2)R_{2,c} +$$
$$4dlG_-^2G_+^4R_1R_2(-l + R_2)R_{2,c} - dG_-^4G_+^4(2l - R_2)(-2l + 3R_2)R_{2,c} + 4d^4lG_-^2G_+R_1R_2^2(-l + R_{2,c}) +$$
$$\left. 4d^4lG_-G_+^2R_1R_2^2(-l + R_{2,c})\right]$$

$$a_{E,y}(\theta,d) = -\Phi_1 dlR_1(2l - R_2)G_-G_+\left[2l^2 + R_2(l - 4R_{2,c})\right] +$$
$$\Phi_2 lR_1(2l - R_2)\left[-lG_-G_+(-2l + 3R_2)R_{2,c} + 2dlG_+R_2(l - R_{2,c}) - 2dlG_-R_2(-l + R_{2,c})\right]$$

$$b_{E,y} = \Phi_1 2dl(G_- - G_+)R_2 \left[dG_-^3 G_+ R_1(2l - R_2)R_{2,c} + dG_-^2 G_+^2 R_1(2l - R_2)R_{2,c} + dG_- G_+^3 R_1(2l - R_2)R_{2,c} + \right.$$
$$\left. d^2 R_1(lG_-^2 G_+(-2l + R_2) + lG_- G_+^2(-2l + R_2) - 2(G_-^3 + G_+^3)(l^2 - R_2 R_{2,c})) \right] +$$
$$\Phi_2 2dl(G_- - G_+)R_2 \left[d^2(G_-^3 G_+(2l - R_2) + G_- G_+^3(2l - R_2) + 2lG_+^2 R_1 R_2 + G_-^2(G_+^2(2l - R_2) + \right.$$
$$2lR_1 R_2))(l - R_{2,c}) + dlG_-^2 G_+ R_1(2l - R_2)R_{2,c} - lG_-^3 G_+ R_1(2l - R_2)R_{2,c} + dlG_- G_+^2 R_1(2l - R_2)R_{2,c} -$$
$$\left. lG_-^2 G_+^2 R_1(2l - R_2)R_{2,c} - lG_- G_+^3 R_1(2l - R_2)R_{2,c} - 2dlG_-^3 R_1(-l + R_2)R_{2,c} - 2dlG_+^3 R_1(-l + R_2)R_{2,c} \right]$$

$$c_{E,y} = \Phi_1 \left[-2d^4 G_-^3 G_+ R_1 R_2^2(l - 2R_{2,c}) - 2d^4 G_- G_+^3 R_1 R_2^2(l - 2R_{2,c}) - 2dG_-^4 G_+^3 R_1(2l - R_2)R_2 R_{2,c} - \right.$$
$$2dG_-^3 G_+^4 R_1(2l - R_2)R_2 R_{2,c} + 2d^3 G_-^4 G_+ R_1 R_2(-2l + R_2)R_{2,c} + 2d^3 G_- G_+^4 R_1 R_2(-2l + R_2)R_{2,c} +$$
$$\left. G_-^4 G_+^4 R_1(2l - R_2)(2l + R_2)R_{2,c} + 4d^4 G_-^4 R_1 R_2(l^2 - R_2 R_{2,c}) - 4d^4 G_+^4 R_1 R_2(-l^2 + R_2 R_{2,c}) \right] +$$
$$\Phi_2 \left[-2d^4 G_-^4 G_+(2l - R_2)R_2(l - R_{2,c}) - 2d^4 G_- G_+^4(2l - R_2)R_2(l - R_{2,c}) - 4d^4 lG_-^3 R_1 R_2^2(l - R_{2,c}) - \right.$$
$$4d^4 lG_+^3 R_1 R_2^2(l - R_{2,c}) + 4dlG_-^4 G_+^2 R_1(l - R_2)R_2 R_{2,c} + 4dlG_-^2 G_+^4 R_1(l - R_2)R_2 R_{2,c} -$$
$$2lG_-^4 G_+^3 R_1(2l - R_2)R_2 R_{2,c} - 2lG_-^3 G_+^4 R_1(2l - R_2)R_2 R_{2,c} + 2d^2 lG_- G_+(G_-^3 + G_+^3)R_1(2l - R_2)R_2 R_{2,c} -$$
$$2d^3 lG_-^3 G_+ R_1 R_2^2 R_{2,c} - 2d^3 lG_- G_+^3 R_1 R_2^2 R_{2,c} + 4dlG_-^3 G_+^3 R_1 R_2^2 R_{2,c} + 4d^3 lG_-^4 R_1 R_2(-l + R_2)R_{2,c} +$$
$$4d^3 lG_+^4 R_1 R_2(-l + R_2)R_{2,c} + dG_-^4 G_+^4(2l - R_2)(-2l + 3R_2)R_{2,c} - 4d^4 lG_-^2 G_+ R_1 R_2^2(-l + R_{2,c}) -$$
$$\left. 4d^4 lG_- G_+^2 R_1 R_2^2(-l + R_{2,c}) \right]$$

Further, the variable $\alpha = \arctan(-x/y)$ is the angle between local horizontal line of the tug and the line connecting the tug and debris.

The control thrusters of the space tug can produce thrust along the local horizontal and local vertical axes

$$\mathbf{U} = U_x \mathbf{e}_x + U_y \mathbf{e}_y \tag{24}$$

The feedback control law of the space tug motion is developed using Eq. (19). However, because during the active debris removal it is necessary to maintain a predetermined relative motion of two bodies, maintaining a balance between the force $\mathbf{P}$ and the Coulomb interaction force, there is a good reason to use the equations of the relative motion. This is the subject of the next subsection. Eq. (19) is used to validate the obtained feedback control law.

Motion of the system in Euler-Hill frame.
Let us consider the motion of the debris relative to the Local-Vertical-Local-Horizontal or Euler-Hill (LVLH) frame $C_1 xy$ [24] (Fig. 1) with the chief (tug) is in a circular orbit. This is a good assumption for GEO debris object tugging. The rectilinear LVLH frame is attached to the space tug. Position of the debris relative to the space tug is described by the column vector

$$\mathbf{d} = \begin{bmatrix} x \\ y \end{bmatrix} \tag{25}$$

The LVLH frame is a non-inertial frame, so the equations of the debris relative to the space tug contains the terms associated with the motion of the LVLH frame relative to the Earth. The equation has the classical form [25]

$$\ddot{x} - 2n\dot{y} - 3n^2 x = a_x$$
$$\ddot{y} + 2n\dot{x} = a_y \tag{26}$$

where n is the orbital rate of the space tug which is changed under the action of the tug's thrust. The change of the orbital rate $\dot{n}$ is approximated as

$$\dot{n} = \frac{P}{m_1 + m_2} \frac{1}{r} \tag{27}$$

where r is the distance from the Earth center to the center of mass of the system. The rate of change of n is close to 0 due to small value of the thrust force P, so the value of $\dot{n}$ is neglected [25]. For example, electric thrusters have thrust output in the micro- to milli-Newton range. For $P = 20\,\text{mN}$ and $m_1 + m_2 = 5000\,\text{kg}$

$$\dot{n} = \frac{20\,\text{mN}}{5000\,\text{kg}} \cdot \frac{1}{35786\,\text{km}} \approx 10^{-13}\,\text{s}^{-2} \tag{28}$$

This value is several orders of magnitude smaller than the magnitude of $n^2 \approx 5 \cdot 10^{-9}\,\text{1/s}^2$ presented in the Eqs. (26).

The right side of the Eq. 26 includes projections of the acceleration produced by the main thruster and control thrusters of the tug and by the electrostatic force

$$\mathbf{a} = \begin{bmatrix} a_x \\ a_y \end{bmatrix} = -\mathbf{F}_{E1}\left(\frac{m_1 + m_2}{m_1 m_2}\right) - (\mathbf{a}_P + \mathbf{u}_x + \mathbf{u}_y) \tag{29}$$

where $\mathbf{a}_P$ is the acceleration of the space tug provided by the main engine thrust $\mathbf{P}$

$$\mathbf{a}_p = \frac{P}{m_1}\begin{bmatrix} 0 \\ 1 \end{bmatrix} = \begin{bmatrix} 0 \\ a_p \end{bmatrix} \tag{30}$$

$\mathbf{u}_x, \mathbf{u}_y$ are the accelerations created by the control engines thrust U_x, U_y

$$u_x = U_x / m_1, \quad u_y = U_y / m_1 \tag{31}$$

Next the relative equations of motion are rewritten using polar coordinates α and d that are more suitable to use during the analysis of relative motion. After substituting $x = d\sin\alpha$, $y = d\cos\alpha$ and their derivatives into the relative equations of motion leads to

$$\ddot{\alpha} = 2\frac{n - \dot{\alpha}}{d}\dot{d} + \frac{3}{2}n^2\sin 2\alpha + \frac{1}{d}\left[(a_p + u_y)\sin\alpha - u_x\cos\alpha\right] + \frac{1}{m_* d}\left(F_{E1,x}\cos\alpha - F_{E1,y}\sin\alpha\right) \tag{32}$$

$$\ddot{d} = d(3n^2\sin^2\alpha - 2n\dot{\alpha} + \dot{\alpha}^2) - (u_y + a_p)\cos\alpha - u_x\sin\alpha - \frac{1}{m_*}\left(F_{E1,x}\sin\alpha + F_{E1,y}\cos\alpha\right) \tag{33}$$

where $m_* = m_1 m_2 / (m_1 + m_2)$ is the reduced mass of the system.

III. Simplified Nonlinear Model (SNM)

Reference [26] shows how to steer a tug for sustainable motion of the system, considering the debris as a simple point-charge model. Now considering the debris as a solid body, an electrostatic tug charge feedback control algorithm should be found to realize a stable debris motion relative to the line connecting mass centers the tug and the debris. The very complicated form of the formulas for the electrostatic torque in Eq. (16) and forces in Eq. (23) make this a challenging task. The following assumptions are used to simplify these formulas and hence the equations of motion described in Eqs. (13), (32) and (33). So, assume the length l of the cylinder body 2 (Fig.1) is substantially less than the distance d between the centers of mass of two bodies

$$\lambda = \frac{l}{d} \ll 1 \tag{34}$$

Then the Coulomb torque in Eq. (16) and forces in Eq. (23) are given by the following approximate formulas:

$$L_E(\theta, d) = \lambda^3 \frac{3R_1}{2k_c d^2}\Phi_1\left(\frac{R_1}{3d}\Phi_1 + \Phi_2\right)\sin 2\theta \tag{35}$$

$$\mathbf{F}_{E1} = \left(F_{E1,x}, F_{E1,y}\right) = -\lambda\frac{7R_1\Phi_1(R_1\Phi_1 - d\Phi_2)}{4k_c d^2}\left(\sin\alpha, \cos\alpha\right) \tag{36}$$

Note that in these formulas it is possible to specify a different degree of expansion in λ if required to account for second or higher order terms. In Eq. (13) the gravity gradient torque in Eq. (15) is excluded, assuming that for GEO orbit this torque is significantly less than the electrostatic torque in Eq. (14).

Substituting Eqs. (35) and (36) into Eqs. (13), (32) and (33), then the simplified nonlinear equations are written as

$$J(\ddot{\theta} - \ddot{\alpha}) = \lambda^3 \frac{3R_1}{2k_c d^2}\Phi_1\left(\frac{R_1}{3d}\Phi_1 + \Phi_2\right)\sin 2\theta \tag{37}$$

$$\ddot{\alpha} = 2\frac{n - \dot{\alpha}}{d}\dot{d} + \frac{3}{2}n^2\sin 2\alpha + \frac{1}{d}\left[(a_p + u_y)\sin\alpha - u_x\cos\alpha\right] \tag{38}$$

$$\ddot{d} = d(3n^2\sin^2\alpha - 2n\dot{\alpha} + \dot{\alpha}^2) - (u_y + a_p)\cos\alpha - u_x\sin\alpha + \lambda\frac{7R_1\Phi_1(R_1\Phi_1 - d\Phi_2)}{4k_c m_* d^2} \tag{39}$$

Equations (38) and (39) are independent of the pitch attitude angle θ and coincide with Eq. (18) in Reference [26]; therefore, in this case, the control laws using Eqs. (21 and (22) can be used from Reference [26]:

$$u_x = c_\alpha\sin\alpha + c_{\dot{\alpha}}\dot{\alpha}, \tag{40}$$

$$u_y = c_{\dot{d}}\dot{d}, \tag{41}$$

The next step is to choose the attitude control law to stabilize the equation of motion in Eq. (37).

IV. Stability of Charged Closed Loop Attitude Motion

Charge Feedback Control Analysis

It is possible to control of the attitude motion using only the magnitude and sign of the electrical charge of the tug. This concept is explored in the following developments for a range of feedback control formulations. The general control law of the electrical change is given as

$$\Phi_1 = \bar{\Phi}_1 \left(1 + \kappa \dot{\theta} f(\theta) \right) \quad \left(\bar{\Phi}_1 < 0 \right) \tag{42}$$

where $f(\theta)$ is the odd periodic function, κ is a constant feedback control parameter.

The odd function $f(\theta)$ is represented as

$$f(\theta) = \sin n\theta, \ (n = 1, 2, ...) \tag{43}$$

Then the electrostatic torque in Eq. **Ошибка! Источник ссылки не найден.**, with accuracy up to terms of the first order ε, is written as

$$L_E \left(\theta, \dot{\theta}, d \right) = \Lambda_1 \sin 2\theta + \Lambda_2 \dot{\theta} \sin 2\theta \sin n\theta \tag{44}$$

$$\Lambda_1 = \lambda^3 \frac{3\bar{\Phi}_1 R_1}{2k_c d^2} \left(\Phi_2 + \frac{R_1}{3d} \bar{\Phi}_1 \right), \ \Lambda_2 = \kappa \lambda^3 \frac{3\bar{\Phi}_1 R_1}{2k_c d^2} \left(\Phi_2 + \frac{2R_1}{3d} \bar{\Phi}_1 \right), \tag{45}$$

Let us assume that the control laws in Eqs. (40) and (41) provide the realization of a stable position of the equilibrium equations (38) and (40).

$$\alpha = 0, d = d_s \tag{46}$$

Eq. (37) is thus rewritten as

$$\ddot{\theta} + \Omega^2 \sin 2\theta = \xi \dot{\theta} \sin 2\theta \sin n\theta \tag{47}$$

with the following simulation parameter definitions:

$$\Omega^2 = -\frac{\Lambda_1 (d = d_s)}{J} = -\lambda^3 \frac{3\bar{\Phi}_1 R_1}{2Jk_c d_s^2} \left(\Phi_2 + \frac{R_1}{3d_s} \bar{\Phi}_1 \right) \tag{48}$$

$$\xi = \frac{\Lambda_2 (d = d_s)}{J} = \kappa \lambda^3 \frac{3\bar{\Phi}_1 R_1}{2Jk_c d_s^2} \left(\Phi_2 + \frac{2R_1}{3d_s} \bar{\Phi}_1 \right) \tag{49}$$

The debris shape to separation distance constraint in Eq. (34) is rewritten into the following inequality expression:

$$\frac{R_1}{3d} << 1 \tag{50}$$

Next the standard assumption is made that

$$\Omega^2 > 0 \tag{51}$$

As can be seen from Eq. (44), this torque becomes zero at the points

$$\theta_* = \pm k \frac{\pi}{2}, \qquad (k = 0, 1, 2, ...) \tag{52}$$

Using the linearized rotational equation in Eq. (47), the points

$$\theta_s = 0 \pm k\pi \tag{53}$$

correspond to the stable equilibrium position, and the points,

$$\theta_u = \frac{\pi}{2} \pm k\pi \tag{54}$$

correspond to the unstable equilibrium position.

In a small neighborhood of the stable equilibrium position

$$\theta_s = 0 \tag{55}$$

which allows Eq. (47) to be reduced to

$$\ddot{\theta} + 2\Omega^2 \theta = 2n \xi \dot{\theta} \theta^2 \tag{56}$$

Next Eq. (56) is rewritten through the use of a dimensionless time $\tau = \sqrt{2}\Omega t$ to a very simple form

$$\theta'' + \theta = \varepsilon \theta' \theta^2 \tag{57}$$

Here the differentiation notation $(\ )' = \frac{d}{d\tau}(\ )$ is used and the following dimensionless small parameter ε is introduced

$$\varepsilon = \frac{\sqrt{2}n\xi}{\Omega} = -\kappa\frac{\lambda n}{d_s}\sqrt{-\frac{2\lambda R_1\Phi_{10}(3d_s\Phi_2 + R_1\Phi_{10})}{Jd_sk_c}} \cdot \frac{3d_s\Phi_2 + 2R_1\Phi_{10}}{3d_s\Phi_2 + R_1\Phi_{10}} \tag{58}$$

For $\varepsilon = 0$ Eq. (57) corresponds to an equation of unperturbed motion

$$\theta'' + \theta = 0 \tag{59}$$

and an energy integral

$$E = \frac{\theta'^2}{2} + \frac{\theta^2}{2} \tag{60}$$

Using the following initial conditions:

$$\tau = 0: \quad \theta = \theta_m, \dot{\theta} = 0 \tag{61}$$

this leads to the initial energy expression of the form

$$E = \frac{\theta_m^2}{2} \tag{62}$$

As a result Eq. (59) has the following general solution:

$$\theta = \theta_m \cos t \tag{63}$$

From Eq. (62) follows an elegantly simple formula for the oscillations amplitudes of the pitch attitude angle

$$\theta_m = \pm\sqrt{2E} \tag{64}$$

The differentiation of Eq. (60) by Eq. (56) yields

$$\frac{dE}{d\tau} = (\theta'' + \theta)\theta' = \varepsilon(\theta'\theta)^2 \tag{65}$$

and

$$\frac{d|\theta_m|}{d\tau} = \varepsilon\frac{(\theta'\theta)^2}{\theta_m} \tag{66}$$

The amplitude $|\theta_m|$ in the closed neighborhood of the equilibrium in Eq. (55) decreases with time if $\varepsilon < 0$. This is satisfied according to Eq. (58) only when the coefficient

$$\kappa > 0 \tag{67}$$

Thus, the formula in Eq. (66) shows that the control law in Eq. (42) leads to a decrease in the amplitude of small oscillations of the debris in the small neighborhood of a stable equilibrium position in Eq. (55). On the other hand, it is easy to see that the factor in Eq. (66)

$$\left[\frac{(\theta'\theta)^2}{\theta_m}\right] \tag{68}$$

for the small vicinity of a stable equilibrium position in Eq. (55) has the third order of smallness. In other words, the oscillations amplitude of the pitch attitude angle in the vicinity of the point in Eq. (55) will decrease very slowly.

Numerical Simulation of the Odd Control Solution

For numerical simulations, system parameters are chosen as in Table 1. The stabilizing control law in Eq. (43) is considered for $n = 1, 2, 3$

$$\Phi_1 = \bar{\Phi}_1\left(1 + \kappa\dot{\theta}\sin n\theta\right) \quad \left(\bar{\Phi}_1 < 0\right) \tag{69}$$

The differential equation in Eq. (56) are integrated with the following initial conditions:

$$\theta_0 = 0.5, \, \dot{\theta}_0 = 0$$

Table 1: Simulation parameters for the detumble control scenario

Parameter	Value	Parameter	Value	Parameter	Value
J, kgm^2	50	l, m	0.5	n	1; 2; 3
$\bar{\Phi}_1$, kW	-20	κ	100	d_s, m	1.997
R_1, m	0.5	$R_{2,a} = R_{2,b}$,	0.5909	$R_{2,c}$, m	0.5909

Figs. 2-4 show the time history (hours) of the pitch attitude angle θ (rad) and the oscillations amplitude $\pm\theta_m$ (rad) for different values n. We note that the parameter has a small impact on the damping of the pitch attitude angle and the detumble is reduced in all cases as predicted by the prior analysis. Using $n=2$, as was done in prior detumble control work by Stevenson [27] for a puller configuration, yields about a 30% reduction in the tumble rate by the end of the simulation. The results when using $n=1$ and $n=3$ yield are very similar results and are less effective than the $n=2$ case. Fig. 5 shows the corresponding tug electrostatic control potentials for . This control potential is still practical to implement as they are similar in magnitude to naturally occurring potentials for GEO objects during emergence from the Earth's shadow.
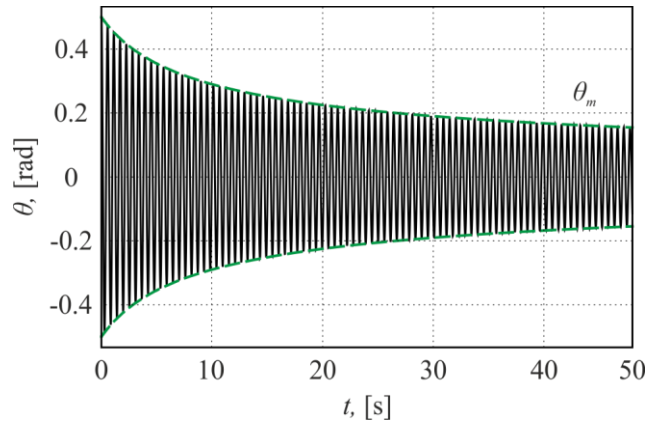
Fig. 2 Time history of the pitch attitude angle θ (solid) and $\theta_m, -\theta_m$ (dotted) for Eq. (57) $\left(n=1\right)$
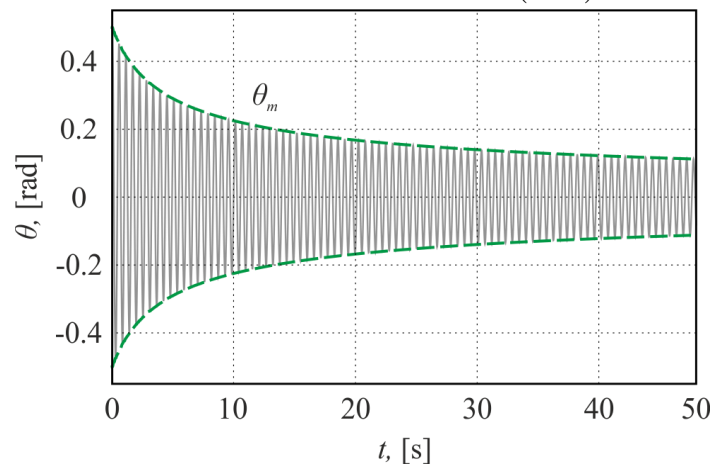
Fig. 3 Time history of the pitch attitude angle θ (solid) and $\theta_m, -\theta_m$ (dotted) for Eq. (57) (n=2)
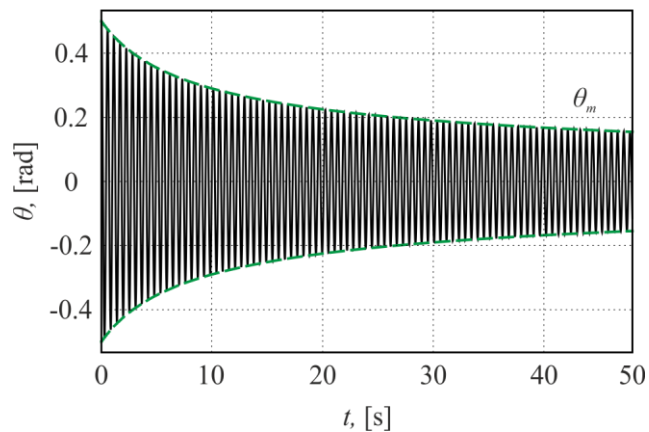
Fig. 4 Time history of the pitch attitude angle (solid) and (dotted) for Eq. (57) (n=3)
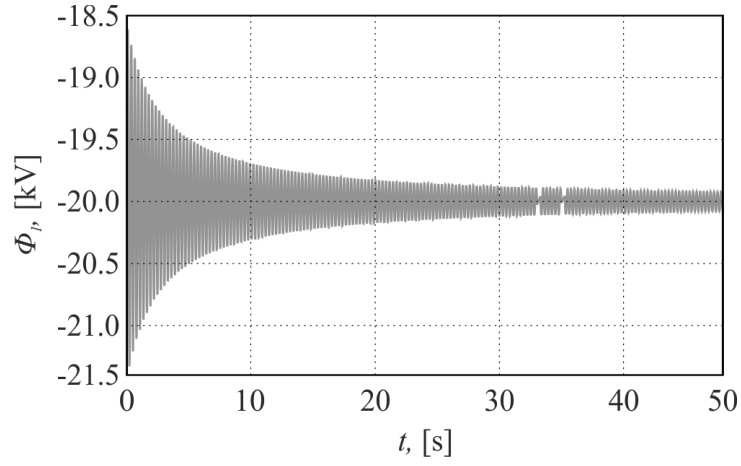
Fig. 5 Time history of the tug electrostatic potential

$$\Phi_1 = \overline{\Phi}_1 \left(1 + \kappa\dot{\theta}\sin n\theta\right) \quad \text{for } n=2$$

V. Numerical Simulation

This section shows with numerical simulations how the parameters of the proposed feedback control affect the stability of the system. The investigation is performed by numerical integration of the initial equations of motion in Eqs. (13), (32) and (33) for the control laws Eqs. (40), (41) and (76).

$$u_x = c_\alpha \sin\alpha + c_{\dot\alpha}\dot\alpha, \tag{77}$$

$$u_y = c_{\dot d}\dot d, \tag{78}$$

$$\Phi_1 = \overline{\Phi}_1 \left(1 + \kappa\dot{\theta}\sin 2\theta\right) \quad \left(\overline{\Phi}_1 < 0\right) \tag{79}$$

The differential Eqs. (13), (32) and (33) are integrated with the following initial conditions

$$\theta_0 = 0.5, \ \dot\theta_0 = 0$$

$$\alpha_0 = 0.5, \dot\alpha_0 = 0 \tag{80}$$

$$d_0 = 2m, \ \dot d_0 = 0 \tag{81}$$

The gravitational toque in Eq. (15) for the GEO orbit is neglected in Eq. (13), considering it small compared with the electrostatic torque in Eq. (14). Additional simulation parameters of the system are given in Table 2.

Table 2. Numerical Simulation parameters

Parameter	Value	Parameter	Value	Parameter	Value
m_1, kg	300	m_2, kg	1000	κ	100
c_α	-0.0001	$c_{\dot\alpha}$	-0.001	$c_{\dot d}$	-0.001
P, mN	5	$J, kg\,m^2$	50	Φ_1, kV	-20

The Figs. 6 - 13 depict the time dependence of the pitch attitude angle θ, the angle between local horizontal line of the tug and the line connecting the tug and debris α, the distance between the space tug and debris d and the charge of the space tug Φ_1 for various the tug's thrust force P.

The simulation results for the tug's thrust force $P=5mN$ are shown in Fig. 6-9. Figures 7 and 8 illustrates that the separation distance and heading are stabilized and the average indicator **Ошибка! Источник ссылки не найден.** is equal to $\lambda = l/d \approx 0.21$ for $t > 3 hours$. Regarding the ability to detumble the debris object while in a pusher configuration, the initial spin rate is first quickly reduced, but then the convergence rate slows down as predicted with the above linearized analysis. The period where the relative motion is still settling to the steady-state location yielded a stronger detumble performance, illustration a direction of future research to investigate this coupled behavior further.

If we take a lighter space tug, a heavier space debris and a less voltage, then as shown in Fig. 10-15, then the initial transient behavior is different, but the convergence properties of the dynamic process practically do not change in comparison with the nominal version (Tabl. 2, Figs. 6-9). This simulations illustrates the robustness of the proposed control solution to system uncertainties. In both cases the detumble control is able to reduce the spin rate while maintaining a stable separation distance in this puller configuration.
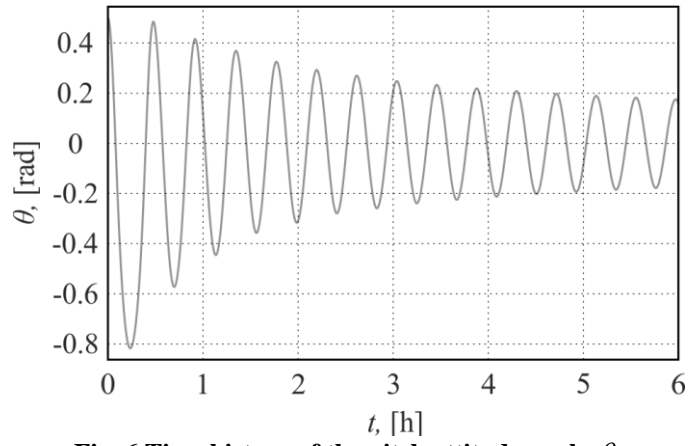
Fig. 6 Time history of the pitch attitude angle θ
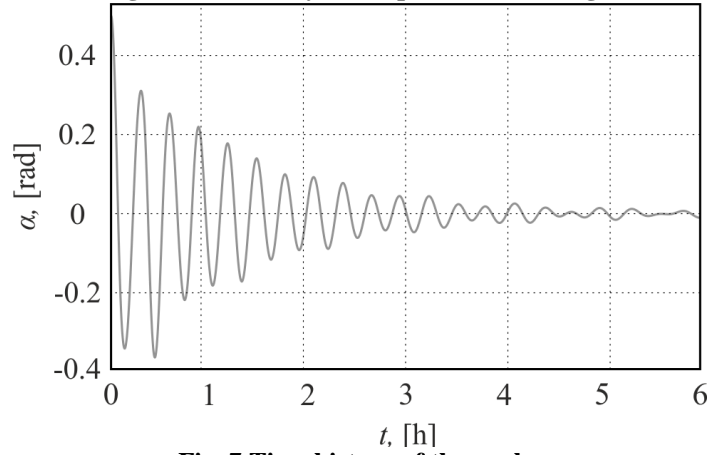
Fig. 7 Time history of the angle α
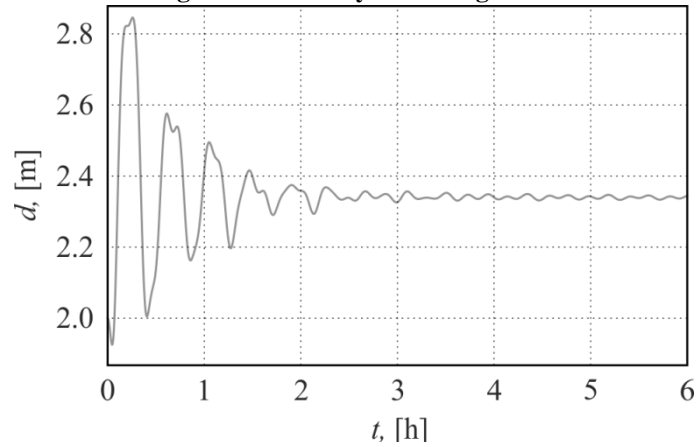
Fig. 8 Time history of the distance between the bodies d
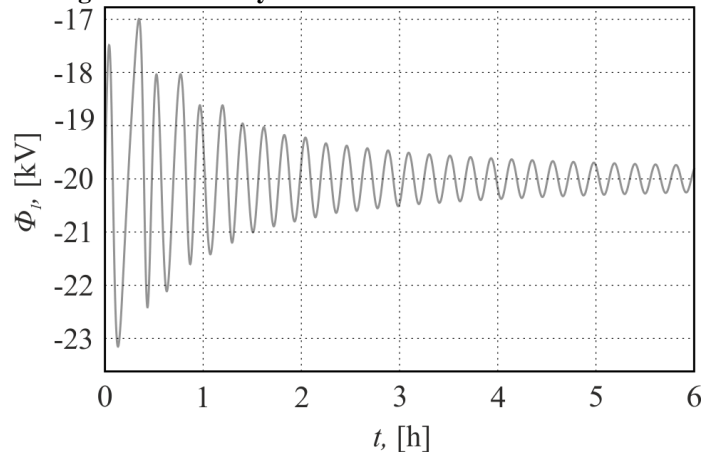
Fig. 9 Time history of the electrical charge of the tug $\Phi_1 = \bar{\Phi}_1 \left(1 + \kappa \dot{\theta} \sin 2\theta \right)$
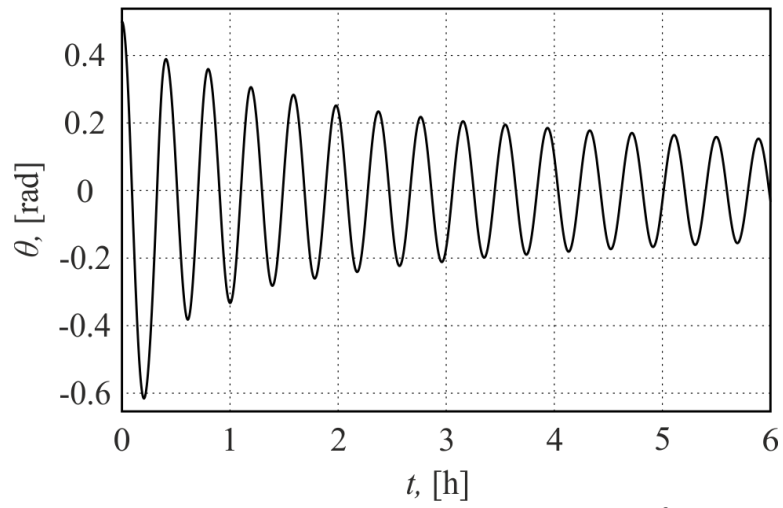
Fig. 10 Time history of the pitch attitude angle θ
for modified system parameters
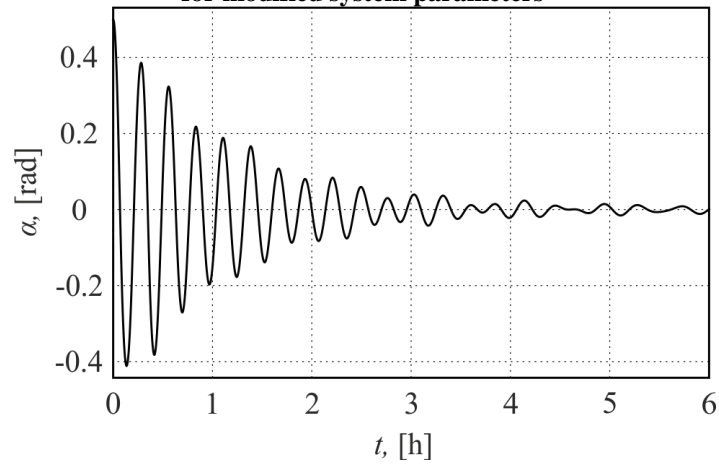
Fig. 11 Time history of the angle α
for modified system parameters
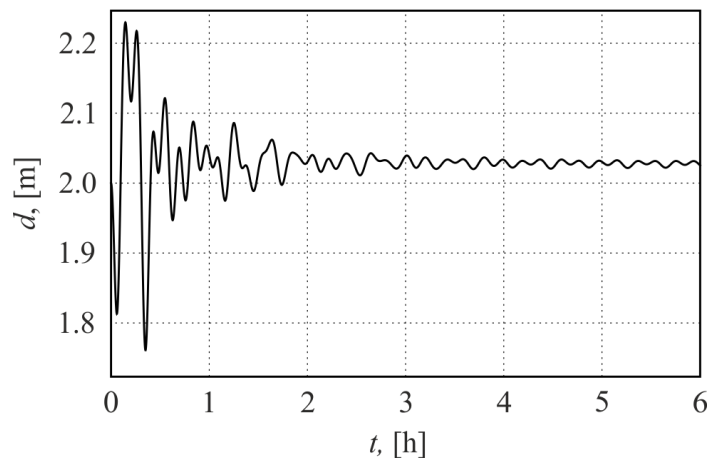
Fig. 12 Time history of the distance between the bodies d **for modified system parameters**
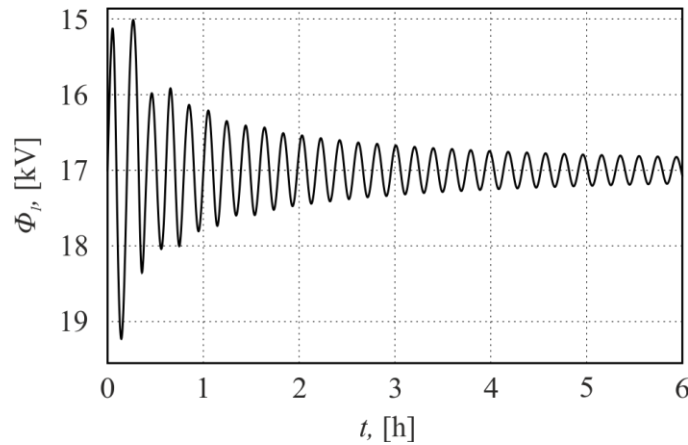
Fig. 13 Time history of the electrical charge of the tug

$$\Phi_1 = \overline{\Phi}_1 \left(1 + \kappa \dot{\theta} \sin 2\theta \right)$$

for modified system parameters

VI. Conclusion

This study explores the relative motion and debris spin rate stability of a pusher electrostatic tug configuration. A simplified electrostatic force and torque formulation is employed to perform an analytical stability analysis for small departure motions. A detumble control formulation is investigated with an feedback function using an odd dependence on the relative rotation angle. In this analytical analysis the nominal separation location is held fixed in an along-track configuration. A challenge with the detumble convergence rate from this control structure is analytically discussed. The numerical simulations illustrate the predicted relative motion and tumble rate stability for a range of tug force configuration, illustrating the robustness to such control parameter variations. Future work could investigate the impact in uncertainties in shape. While this study considers a range of mass, inertia and control potentials, the debris shape is assumed to be cylindrical. If the modeled and actual shape differ than the torque modeling errors could impact both the performance and convergence of the detumble control. Further, this work is specific to planar rotation of the debris. It would be interesting to expand this analysis to general three-dimensional relative rotation and modify the control solution for such a scenario.

References

[1] Liou, J.-C., Johnson, N., and Hill, N., "Controlling the growth of future LEO debris populations with active debris removal," *Acta Astronautica*, Vol. 66, No. 5-6, 2010, pp. 648 – 653, doi:10.1016/j.actaastro.2009.08.005.

[2] Oltrogge, D. L., Alfano, S., Law, C., Cacioni, A., and Kelso, T. S., "A Comprehensive Assessment of Collision Likelihood in Geosynchronous Earth Orbit," *International Astronautical Congress*, Adelaide, Australia, Sept. 25–29 2017.

[3] Anderson, P. V. and Schaub, H., "Local Debris Congestion in the Geosynchronous Environment With Population Augmentation," *Acta Astronautica*, Vol. 94, No. 2, Feb. 2014, pp. 619–628, doi:10.1016/j.actaastro.2013.08.023.

[4] Binz, C. R., Davis, M. A., Kelm, B. E., and Moore, C. I., "Optical Survey of the Tumble Rates of Retired GEO Satellites," *Advanced Maui Optical and Space Surveillance Technologies Conference*, Maui, Hawaii, Sept. 9–12 2014.

[5] Bombardelli, C. and Pelaez, J., "Ion Beam Shepherd for Contactless Space Debris Removal," *AIAA Journal of Guidance, Control, and Dynamics*, Vol. 34, No. 3, May–June 2011, pp. 916–920, doi:10.2514/1.51832.

[6] Kumar, R. and Sedwick, R. J., "Despinning Orbital Debris Before Docking Using Laser Ablation," *AIAA Journal of Spacecraft and Rockets*, Vol. 52, No. 4, 2015, pp. 1129–1134, doi:10.2514/1.A33183

[7] Schaub, H. and Moorer, D. F., "Geosynchronous Large Debris Reorbiter: Challenges and Prospects," *The Journal of the Astronautical Sciences*, Vol. 59, No. 1–2, 2014, pp. 161–176, doi:10.1007/s40295-013- 0011-8.

[8] Daan Stevenson, ``Remote Spacecraft Attitude Control by Coulomb Charging," Ph.D. Dissertation, Aerospace Engineering Sciences Department, University of Colorado, Boulder, CO, May 2015.

[9] Shibata, T., Bennett, T., and Schaub, H., "Prospects of a Hybrid Magnetic/Electrostatic Sample Con- tainer Retriever," *9th International Workshop on Satellite Constellations and Formation Flying*, Boulder, CO, June 19–21 2017, Paper No. IWSCFF 17-15.

[10] Hogan, E. and Schaub, H., "Relative Motion Control for Two-Spacecraft Electrostatic Orbit Corrections," *AIAA Journal of Guidance, Control, and Dynamics*, Vol. 36, No. 1, Jan. – Feb. 2013, pp. 240–249, doi:10.2514/1.56118.

[11] Bennett, T. and Schaub, H., "Touchless Electrostatic Detumble Of A Representative Box-And-Panel Spacecraft Configuration," *European Conference on Space Debris*, ESOC, Darmstadt, Germany, April, 18–21 2017.

[12] E. G. Mullen, M. S. Gussenhoven, D. A Hardy, T. A. Aggson, and B. G. Ledley. SCATHA survey of high-voltage spacecraft charging in sunlight. *Journal of Geophysical Research*, 91(A2):1474–1490, 1986.

[13] Joseph F. Fennell and James L. Roeder. HEO satellite surface and frame charging and SCATHA low-level frame charging. Technical Report TR-2007(8570)-1, The Aerospace Corporation, El Segundo, CA, Nov. 15 2007.

[14] Joseph F. Fennell, H. C. Koons, M. S. Leung, and P. F. Mizera. A review of SCATHA satellite results: Charging and discharging. Technical report, Space Division Air Force Systems Command, Los Angeles Air Force Station, Aug. 1985.

[15] R. C. Olsen and E. C. Whipple. Analysis of differential and active charging phenomena on ATS-5 and ATS-6. Technical report, NASA, 1980.

[16] E. C. Whipple and R. C. Olsen. Importance of differential charging for controlling both natural and induced vehicle potentials on ats-5 and ats-6. In *Proceedings of the 3rd Spacecraft Charging Technology Conference*, page 887, Nov. 12–14 1980. NASA Conference Publication 2182.

[17] Daan Stevenson and Hanspeter Schaub. Multi-sphere method for modeling electrostatic forces and torques. *Advances in Space Research*, 51(1):10–20, Jan. 2013.

[18] Daan Stevenson and Hanspeter Schaub. Optimization of sphere population for electrostatic multi sphere model. *IEEE Transactions on Plasma Science*, 41(12):3526–3535, Dec. 2013.

[19] Philip Chow, Joseph Hughes, Trevor Bennett, and Hanspeter Schaub. Automated sphere geometry optimization for the volume multi-sphere method. In *AAS/AIAA Spaceflight Mechanics Meeting*, pages 2223–2240, Napa Valley, California, Feb. 14–18 2016. Paper No. AAS-16- 472.

[20] Gabriel Ingram, Joseph Hughes, Trevor Bennett, Christine Reilly, and Hanspeter Schaub. Autonomous volume multi-sphere-model development using electric field matching. In *AAS Spaceflight Mechanics Meeting*, San Antonio, TX, Feb. 5–9 2017. Paper AAS 17-451.

[21] W. R. Smythe. *Static and Dynamic Electricity*. McGraw–Hill, 3rd edition, 1968.

[22] Fuzhen Zhang. The Schur Complement and Its Applications. Springer, Boston, MA, 2005.

[23] S. Wolfram, S., The Mathematica Book, 5th ed., Cambridge University Press, Cambridge, 2003.

[24] Alfriend, K. T., Vadali, S. R., Gurfil, P., How, J. P., and Breger, L. S., "Linear Equations of Relative Motion," Spacecraft Formation Flying, Butterworth-Heinemann, Oxford, England, U.K., 2010, pp. 83–121. doi:10.1016/B978-0-7506-8533-7.00210-4

[25] Hogan, E. A. and Schaub, H., "Attitude Parameter Inspired Relative Motion Descriptions for Relative Orbital Motion Control," *AIAA Journal of Guidance, Control, and Dynamics*, Vol. 37, No. 3, 2014, pp. 741–749, doi:10.2514/1.60626.

[26] V. S. Aslanov, V. V. Yudintsev, Motion Control of Space Tug During Debris Removal by a Coulomb Force. Journal of Guidance, Control, and Dynamics, 2018, March 22, 2018. doi: 10.2514/1.G003251

[27] Schaub, H. and Stevenson, D., "Prospects Of Relative Attitude Control Using Coulomb Actuation," *Journal of the Astronautical Sciences*, Vol. 60, No. 3, 2013, pp. 258–277, doi:10.1007/s40295-015-0048-y.